Available online at www.eccomasproceedia.org
Eccomas Proceedia UNCECOMP (2025) 364-382

ECCOMAS
Proceedia

UNCECOMP 2025
6th ECCOMAS Thematic Conference on
Uncertainty Quantification in Computational Science and Engineering
M. Papadrakakis, V. Papadopoulos, G. Stefanou (eds.)
Rhodes Island, Greece, 15-18 June 2025

STOCHASTIC FINITE ELEMENT ANALYSIS OF CONCRETE BEAMS

Leontios Kotropoulos*, George Stefanou

Department of Civil Engineering, Aristotle University of Thessaloniki
University Campus, 54124 Thessaloniki, Greece
leoskotrop@gmail.com, gstefanou@civil.auth.gr

Abstract

In recent years, the rapid advancement of computers and their capabilities has enabled the solution of complex realistic problems using numerical methods, such as the finite element method (FEM). The classical deterministic FEM ignores the inherent uncertainty in the problem's parameters. This unutilized information is taken into account in the stochastic finite element method (SFEM), which is an extension of the classical method, incorporating stochastic analysis to handle uncertainties. In the framework of SFEM, the finite elements are characterized by random properties described by random variables. In this way, a more refined and accurate model of the problem is created, although this leads to an increase in computational cost.

The aim of the present work is the application of SFEM for the analysis of two concrete structures and the extraction of useful conclusions that can lead to safer and more cost-effective designs, as well as to the improvement of safety factors in construction codes. To this end, the mesoscale random fields of the elasticity tensor of concrete are determined from the reconstructed microstructure of a cubic specimen. Additionally, their statistical characteristics are computed and sample functions are generated using the spectral representation method and translation field theory, in order to examine the response variability of the above structures and to understand the effect of the random microstructure on their macroscopic behavior.

Keywords: Concrete, Mesoscale random fields, Response variability.

ISSN:2623-3339 © 2025 The Authors. Published by Eccomas Proceedia.
Peer-review under responsibility of the organizing committee of UNCECOMP 2025.
doi: 10.7712/120225.12362.21413

1 INTRODUCTION

Concrete is by far the dominant material in construction. It is estimated that the current global production of concrete amounts to approximately 11 billion tons per year, making it the most widely produced material in the world today. No other material, apart from water, is consumed by humans in such astonishing quantities. Additionally, concrete is the primary material that determines the economic development of a region, as most infrastructure projects are built with it. However, its highly heterogeneous and complex microstructure makes it very difficult to reliably predict its behavior, since theoretical models and analytical methods in mechanics of materials are insufficient when it comes to concrete structures [1].

In this work, the response variability of two concrete structures is computed using stochastic finite elements based on mesoscale random fields of the elasticity tensor, which are derived from the reconstructed microstructure of a cubic specimen [2]. To achieve this, the statistical characteristics of these fields are evaluated [3] and sample functions are generated using the spectral representation method in conjunction with translation field theory [4,5]. The objective is to assess the effect of the random microstructure on the macroscopic behavior of the above structures, with the ultimate goal of extracting useful conclusions that can lead to safer and more cost-effective designs, as well as to the improvement of safety factors in construction codes.

The paper is organized as follows: In Section 2, the methodology followed for determining the mesoscale random fields of the elasticity tensor of concrete from the reconstructed microstructure of a cubic specimen is analyzed. Section 3 focuses on the generation of sample functions and the examination of the response variability of two concrete structures. The key conclusions derived are presented in Section 4.

2 RANDOM FIELDS OF THE ELASTIC PROPERTIES OF CONCRETE

In this section, the methodology followed in the recent publication by Stefanou et al. [2] for determining the spatial variation of the elastic properties of concrete at various scales is presented, taking into account its highly heterogeneous and complex microstructure. From the computed tomography of a cubic concrete specimen, its microstructure is reconstructed and the mesoscale random fields of the elasticity tensor are computed by applying the moving window method in conjunction with the computational homogenization process. The analysis of the statistical characteristics of the mesoscale random fields enables the investigation of the effect of the random microstructure on the macroscopic behavior of concrete.

2.1 Computed tomography

Computed tomography is an imaging method for visualizing the internal structure of an object using X-rays. More specifically, a radiation source rotates around the object and its attenuation is measured by a series of detectors positioned diametrically opposite, as shown in Figure 1. Upon completing a full rotation, automated algorithms generate a two-dimensional cross-sectional image of the object, known as a tomographic image. When a sufficient number of consecutive tomographic images of the object are collected, they can be combined to reconstruct its three-dimensional internal structure.

Each pixel of the tomographic image represents the measured attenuation value of the radiation, which is converted through a linear transformation into the corresponding HU value on the Hounsfield scale. The Hounsfield scale is a system for quantifying the density of an object, where distilled water under standard pressure and temperature corresponds to $0\ \mathrm{HU}$, while air under the same conditions corresponds to $-1000\ \mathrm{HU}$.

Although computed tomography was initially developed and applied for medical purposes, the gradual increase in its availability and reduction in cost today have expanded its use to other fields, such as the study of the microstructure of heterogeneous materials.

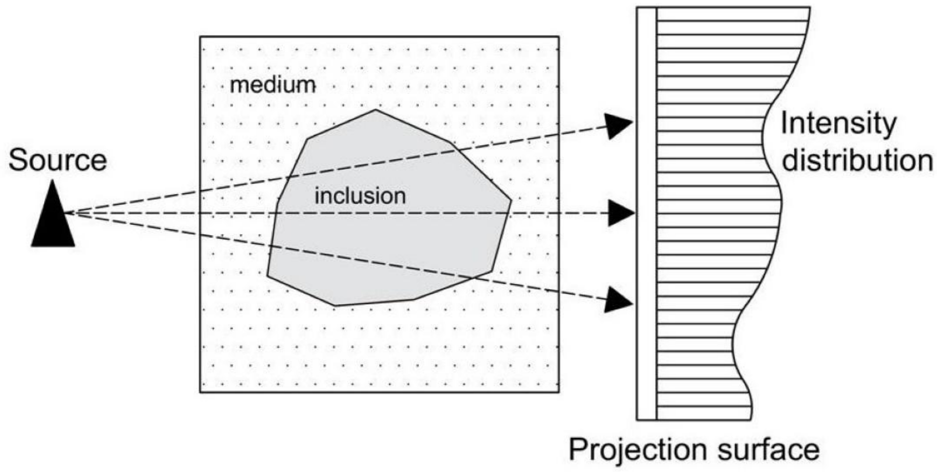

Figure 1: Source-detector pair and radiation attenuation.

2.2 Computational homogenization

Computational homogenization is a process used to replace a heterogeneous material with an equivalent homogeneous one by determining its effective properties. This approach offers an efficient alternative for analyzing heterogeneous materials, as the computational cost is significantly reduced compared to directly simulating the microstructure at the macroscale. The effective properties describe the macroscopic behavior of the heterogeneous material and are linked to its microstructural characteristics through Hill's energy condition, which is also referred to as Hill's macro-homogeneity condition by some researchers.

2.2.1 Representative and statistical volume element

In the context of computational homogenization, a representative volume element (RVE) is considered, which sufficiently captures the microstructure of a heterogeneous material. The RVE must be large enough to incorporate all essential microstructural characteristics, while remaining small enough to allow efficient computational handling.

According to Hashin [6], the determination of the RVE is based on the assumption of statistical homogeneity, which states that the statistical characteristics of a heterogeneous material are similar throughout its extent. In the case of heterogeneous materials with a periodic or nearly periodic microstructure, the RVE can be explicitly defined, whereas for heterogeneous materials with a random microstructure, the RVE is determined approximately.

According to Hill [7], the existence of the RVE requires a separation of scales in the form:

$$d \ll L \ll L_{macro} \tag{1}$$

where d the characteristic dimension of the microstructure, such as the average size of the aggregates, L the characteristic dimension of the RVE at the mesoscale and L_{macro} the characteristic dimension of the problem at the macroscale. Figure 2 depicts an illustration of scale separation.

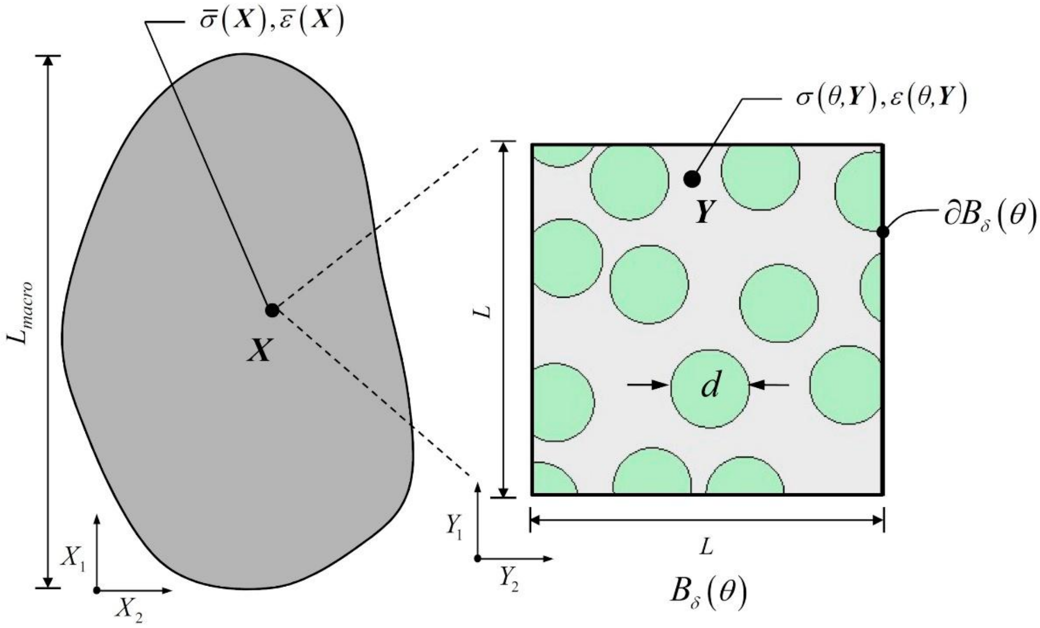

Figure 2: Illustration of scale separation.

The RVE is characterized by constant and deterministic properties. To account for the spatial variation of properties at the mesoscale, the concept of the statistical volume element (SVE) is introduced [8,9]. The SVE is always smaller than the corresponding RVE and is described by the non-dimensional parameter $\delta = L/d$ with $\delta \in [1,\infty]$, which is called the scale factor. The properties derived from an SVE are referred to as apparent properties. When $\delta \to \infty$, the SVE approaches the corresponding RVE and the apparent properties converge to the effective properties.

2.2.2 Computation of the apparent elasticity tensor

Let a random mesoscale realization of the microstructure of a heterogeneous material $B_\delta(\theta)$, which is defined in a coordinate system Y. The stress and strain fields, expressed as a superposition of means ($\bar{\sigma}$ and $\bar{\varepsilon}$) and zero-mean fluctuations (σ' and ε'), are written as:

$$\sigma(\theta,Y) = \bar{\sigma} + \sigma'(\theta,Y) \qquad \varepsilon(\theta,Y) = \bar{\varepsilon} + \varepsilon'(\theta,Y) \tag{2}$$

The means of stress and strain tensors at some point X of the macroscale are computed as:

$$\bar{\sigma}(X) = \frac{1}{V_\delta} \int_{B_\delta(\theta)} \sigma(\theta,Y)\, dV_\delta \qquad \bar{\varepsilon}(X) = \frac{1}{V_\delta} \int_{B_\delta(\theta)} \varepsilon(\theta,Y)\, dV_\delta \tag{3}$$

The volume average of the strain energy is given by:

$$\bar{U} = \frac{1}{2V_\delta} \int_{B_\delta(\theta)} \sigma(\theta,Y) : \varepsilon(\theta,Y)\, dV_\delta = \frac{1}{2}\overline{\sigma : \varepsilon} = \frac{1}{2}\bar{\sigma} : \bar{\varepsilon} + \frac{1}{2}\overline{\sigma' : \varepsilon'} \tag{4}$$

where the notation $\sigma : \varepsilon$ represents $\sigma_{ij}\varepsilon_{ij}$. For $\delta \to \infty$ the term $\overline{\sigma' : \varepsilon'}$ becomes negligible and it follows that:

$$\overline{\sigma : \varepsilon} = \bar{\sigma} : \bar{\varepsilon} \tag{5}$$

Equation (5) is known as Hill's energy condition and is also valid when the following constraint is satisfied:

$$\int_{\partial B_\delta} \left(t-\bar{\sigma}n\right)\left(u-\bar{\varepsilon}Y\right)dS = 0 \tag{6}$$

where t the traction vector and u the displacement vector. Equation (6) is a priori satisfied by the following boundary conditions:

- Uniform strains (otherwise known as kinematic, essential or Dirichlet)
- Uniform stresses (otherwise known as static, natural or Neumann)
- Uniform orthogonal-mixed
- Periodic

The elasticity tensor, being a 4th order tensor, contains $3^4 = 81$ components, which are reduced to 21 independent components due to symmetry. The matrix form of the elasticity tensor is given by:

$$C = \begin{bmatrix} C_{11} & C_{12} & C_{13} & C_{14} & C_{15} & C_{16} \\ C_{21} & C_{22} & C_{23} & C_{24} & C_{25} & C_{26} \\ C_{31} & C_{32} & C_{33} & C_{34} & C_{35} & C_{36} \\ C_{41} & C_{42} & C_{43} & C_{44} & C_{45} & C_{46} \\ C_{51} & C_{52} & C_{53} & C_{54} & C_{55} & C_{56} \\ C_{61} & C_{62} & C_{63} & C_{64} & C_{65} & C_{66} \end{bmatrix} \tag{7}$$

In order to determine the apparent elasticity tensor, it is necessary to impose a prescribed uniform strain tensor $\bar{\varepsilon} = \left[\bar{\varepsilon}_1 \quad \bar{\varepsilon}_2 \quad \bar{\varepsilon}_3 \quad \bar{\varepsilon}_4 \quad \bar{\varepsilon}_5 \quad \bar{\varepsilon}_6\right]^T$ on the boundary nodes of the discretized microstructure model through the following uniform displacements:

$$u_b = D_b^T \bar{\varepsilon} \tag{8}$$

where D_b a geometric matrix which depends on the coordinates Y_1, Y_2, Y_3 of the boundary node b and is defined as:

$$D_b = \frac{1}{2}\begin{bmatrix} 2Y_1 & 0 & 0 \\ 0 & 2Y_2 & 0 \\ 0 & 0 & 2Y_3 \\ Y_2 & Y_1 & 0 \\ 0 & Y_3 & Y_2 \\ Y_3 & 0 & Y_1 \end{bmatrix} \tag{9}$$

The apparent elasticity tensor is now computed as:

$$C_\delta\left(\theta\right) = \frac{1}{V_\delta} D\tilde{K}_{bb} D^T \tag{10}$$

where $\tilde{K}_{bb} = K_{bb} - K_{bi}K_{ii}^{-1}K_{ib}$ the condensed stiffness matrix resulting from the separation of the internal nodes i and the boundary nodes b and $D = \left[D_1 \quad D_2 \quad \ldots\right]$ a matrix containing the geometric matrices D_b of the boundary nodes b [10].

2.3 Determination of mesoscale random fields

The determination of the mesoscale random fields of the elasticity tensor of concrete is achieved through the application of the moving window method to a cubic specimen, whose microstructure has been reconstructed based on a set of tomographic images.

2.3.1 Reconstruction of concrete microstructure

The cubic concrete specimen used had dimensions of approximately $136.724 \times 136.724 \times 131.25\ \text{mm}^3$. From its computed tomography with a constant slice thickness of $0.625\ \text{mm}$, 211 tomographic images were obtained with a resolution of 281×281 pixels, meaning a pixel spacing of $0.4883 \times 0.4883\ \text{mm}^2$. Figure 3 depicts a tomographic image of the cubic concrete specimen.

These data are utilized for the reconstruction of its microstructure, which is divided into a set of SVEs, as shown in Figure 4, by applying the moving window method. Each SVE is discretized with hexahedral elements corresponding to the voxels of the reconstructed microstructure. In order to reduce the computational cost, the hexahedral elements consist of a grid of $2 \times 2 \times 2$ voxels. At the integration points of the hexahedral elements, the appropriate material is assigned depending on the HU values of these points, which are computed based on the corresponding nodal quantities through the shape functions.

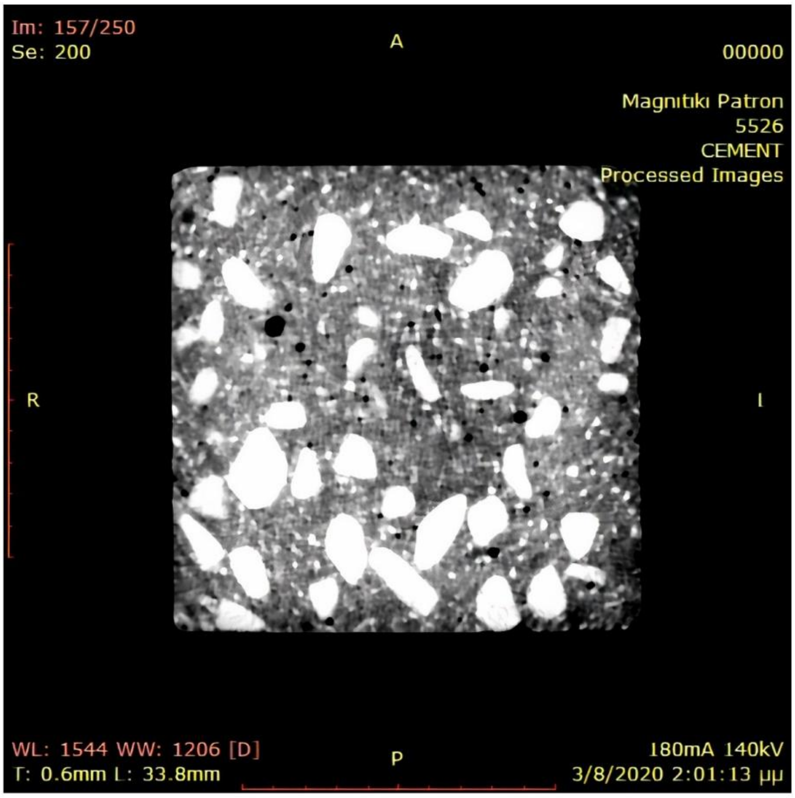

Figure 3: Tomographic image of the cubic concrete specimen.

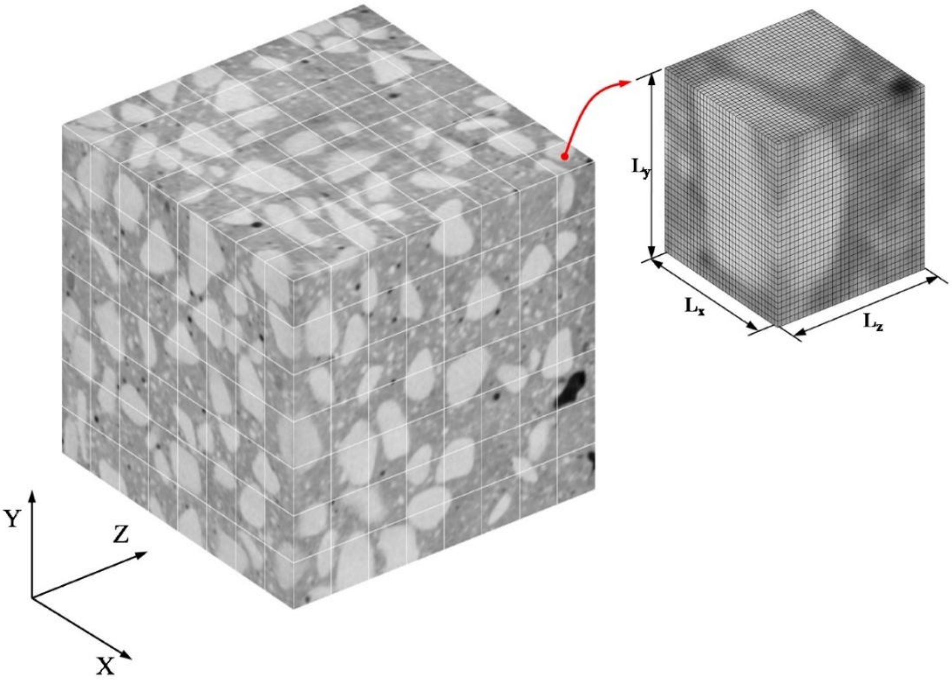

Figure 4: Reconstructed microstructure of the cubic concrete specimen, which has been divided into a set of SVEs.

The distinction of concrete constituents lies in defining representative HU value ranges for each of them. More specifically, for the pores, cement and aggregates the ranges $[-960, 800]$, $[800, 2000]$ and $[2000, 2974]$ are selected respectively, as shown in Figure 5. Additionally, for the cement the modulus of elasticity and Poisson's ratio are considered to be 20 GPa and 0.2 respectively, while for the aggregates the same properties are considered to be 100 GPa and 0.2 respectively. The pores are modeled as an almost incompressible material with a modulus of elasticity equal to 1% of that of cement, meaning a modulus of elasticity and Poisson's ratio of 0.2 GPa and 0.45 respectively.

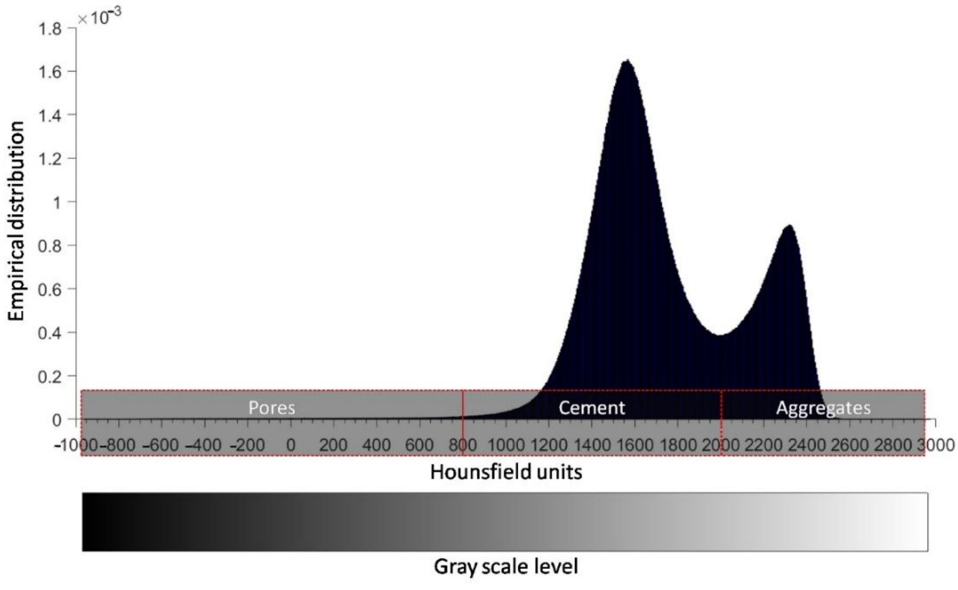

Figure 5: Empirical distribution of HU values.

2.3.2 Moving window method

In the moving window method, an initial window of dimensions $L_x \times L_y \times L_z$ is shifted with a fixed step $\Delta\xi$ in all three directions, fully covering the microstructure. In this way, a set of windows is extracted, each containing a small portion of the microstructure. For every window, the apparent properties are computed through the procedure described in Section 2.2.2. These properties are then combined with the positions of the window centers to form the corresponding random fields. Figure 6 depicts an illustration of the moving window method.

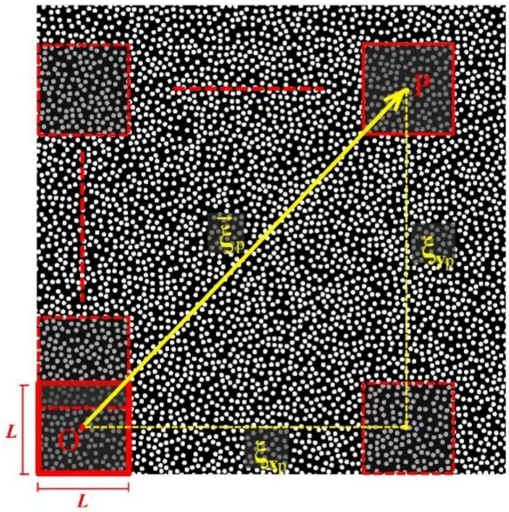

Figure 6: Illustration of the moving window method.

From the random fields, histograms of their values can be obtained and their spatial correlation functions can be determined for every lag $\left(\xi_x, \xi_y, \xi_z\right)$ as:

$$\begin{gathered}\rho_A^B\left(\xi_x, \xi_y, \xi_z\right) = \frac{1}{n_{wx} n_{wy} n_{wz} - 1} \sum_{i=0}^{n_{wx}} \sum_{j=0}^{n_{wy}} \sum_{k=0}^{n_{wz}} \\ \left(\frac{A\left(x_i, y_j, z_k\right) - \mu_A}{\sigma_A}\right)\left(\frac{B\left(x_i + \xi_x, y_j + \xi_y, z_k + \xi_z\right) - \mu_B}{\sigma_B}\right) \\ -n_{wx}\Delta\xi \le \xi_x \le n_{wx}\Delta\xi, -n_{wy}\Delta\xi \le \xi_y \le n_{wy}\Delta\xi, -n_{wz}\Delta\xi \le \xi_z \le n_{wz}\Delta\xi\end{gathered} \tag{11}$$

where μ_A, μ_B the mean values and σ_A, σ_B the standard deviations of quantities A, B respectively. When $A \equiv B$, ρ_A^B denotes auto-correlations, otherwise cross-correlations are defined.

It is noted that the moving window step was selected equal to its size to avoid extracting overlapping windows. The examined mesoscale sizes, the dimensions of the moving window and the total number of SVEs are provided in Table 1.

δ_i	L_x x L_y x L_z (mm^3)	No. SVEs
δ_1	4.88 x 4.88 x 6.25	16464
δ_2	9.77 x 9.77 x 8.75	2940
δ_3	19.53 x 19.53 x 18.75	343
δ_4	27.34 x 27.34 x 26.25	125

Table 1: Examined mesoscale sizes, dimensions of the moving window and total number of SVEs.

2.3.3 Results

In this work, the mean xy plane of the three-dimensional concrete specimen is considered and the two-dimensional random fields of the elasticity components C_{11} and C_{44} are computed for all examined mesoscale sizes. These fields are depicted in Figures 7 and 8. The elasticity components C_{11} and C_{44} represent the axial and shear stiffness respectively and are measured in GPa. Lengths are measured in mm.

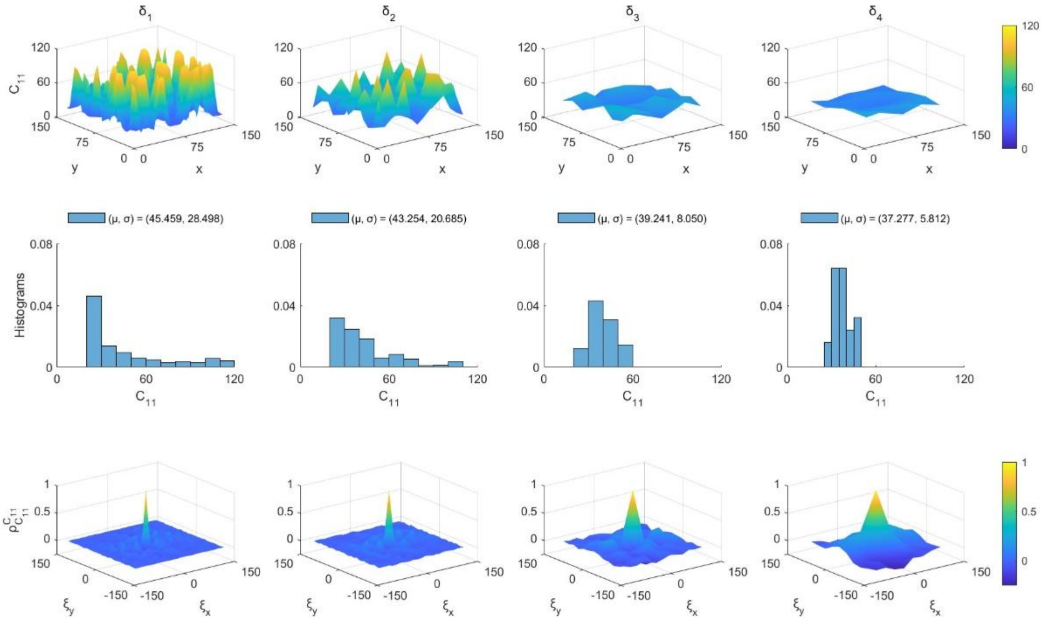

Figure 7: Random fields of the elasticity component C_{11}.

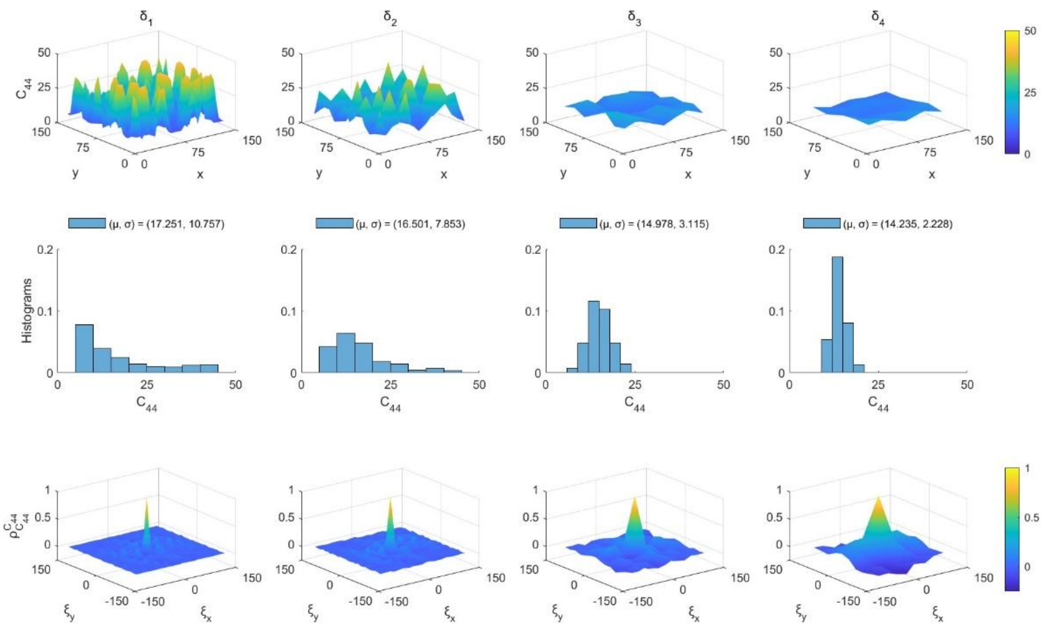

Figure 8: Random fields of the elasticity component C_{44}.

Figure 9 depicts the cross-correlations between the elasticity components C_{11} and C_{44} for lag values along x (ξ_x, $\xi_y = 0$) and y ($\xi_x = 0$, ξ_y), while Figure 10 depicts their scatter plots.

From Figure 10, it follows that the elasticity components C_{11} and C_{44} exhibit a strong correlation with each other, as expected.

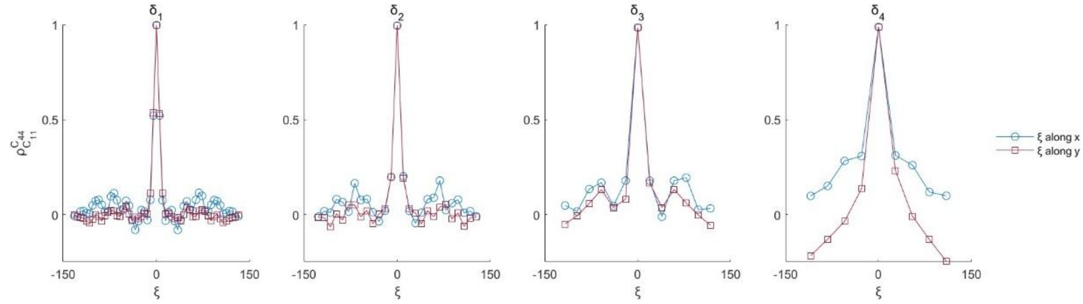

Figure 9: Cross-correlations between the elasticity components C_{11} and C_{44} for lag values along x (ξ_x, $\xi_y = 0$) and y ($\xi_x = 0$, ξ_y).

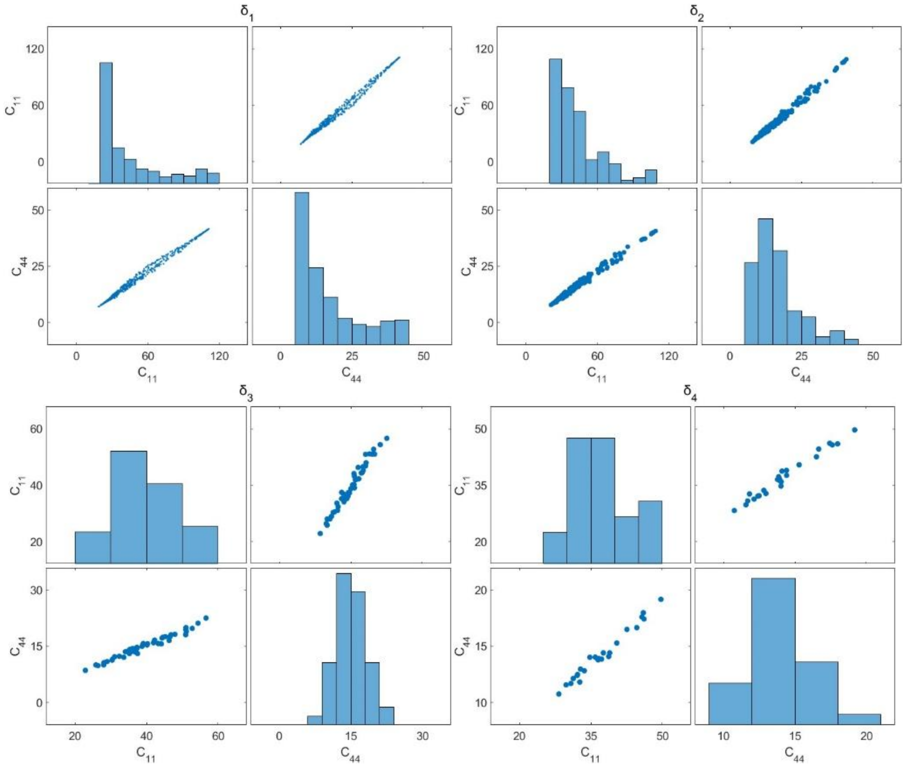

Figure 10: Scatter plots of the elasticity components C_{11} and C_{44}.

The correlation lengths of the random fields of the elasticity components C_{11} and C_{44} are obtained by fitting a predefined correlation model to their auto-correlations, as shown in Figures 11 and 12. In this work, the squared exponential model is used, as it represents a realistic choice for concrete and is given by:

$$R_{ff}\left(\xi_x, \xi_y\right) = \sigma^2 \exp\left[-\left(\frac{\xi_x}{b_x}\right)^2 - \left(\frac{\xi_y}{b_y}\right)^2\right] \tag{12}$$

where b_x, b_y the parameters which are proportional to the correlation lengths of the random fields along the x, y axes respectively.

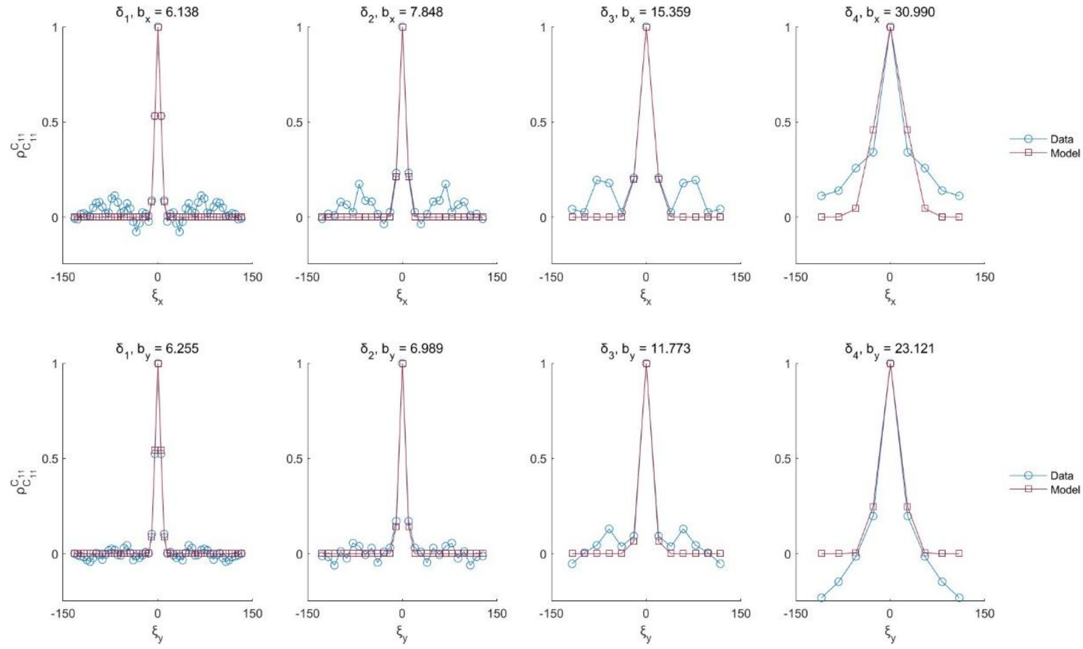

Figure 11: Fitting of the squared exponential model to the auto-correlations of the elasticity component C_{11}.

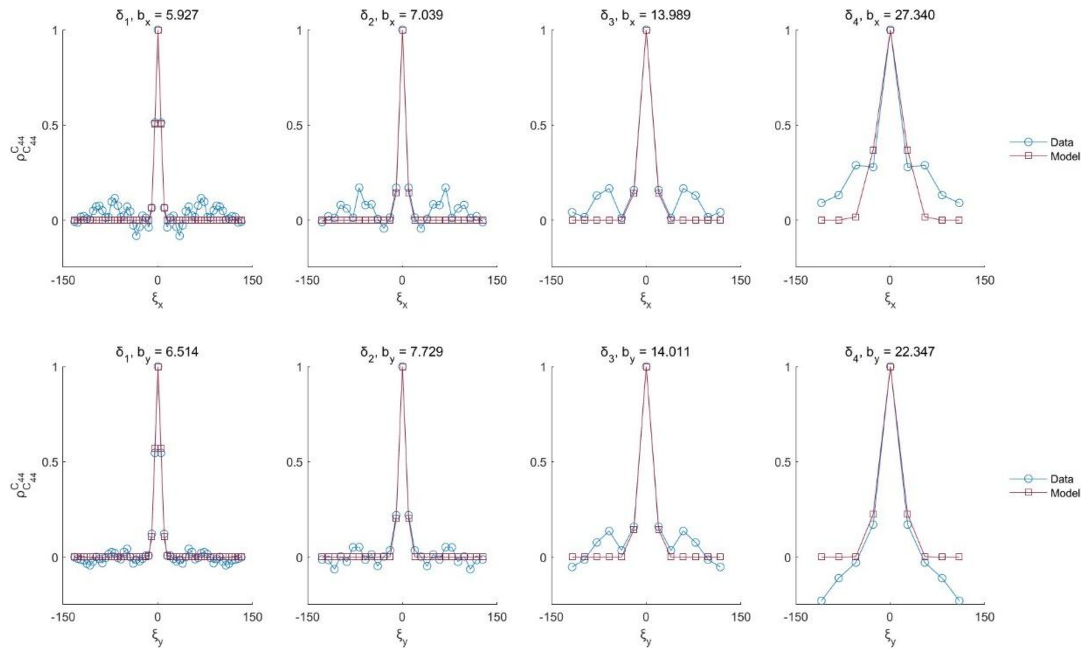

Figure 12: Fitting of the squared exponential model to the auto-correlations of the elasticity component C_{44}.

Additionally, the fitting of both the normal and the lognormal distribution to the histograms of the elasticity components C_{11} and C_{44} is examined, as shown in Figures 13 and 14. It is observed that the lognormal distribution provides a satisfactory approximation of these histograms and therefore non-Gaussian fields are required for the simulation of the random fields of the elasticity components C_{11} and C_{44}, particularly at smaller scales. Another reason for preferring the lognormal distribution is that it eliminates the possibility of negative values for the elasticity components C_{11} and C_{44}.

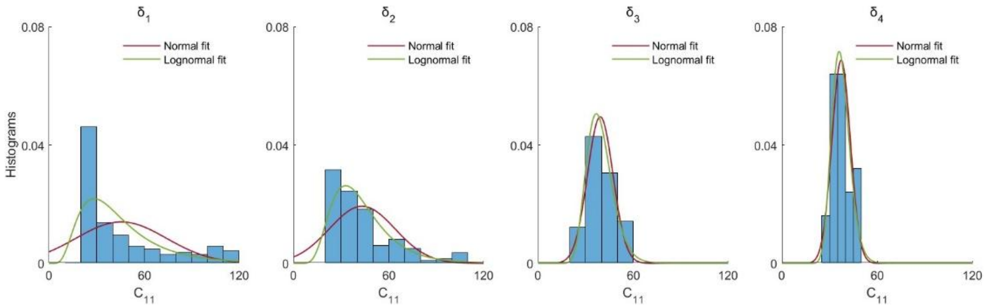

Figure 13: Fitting of both the normal and the lognormal distribution to the histograms of the elasticity component C_{11}.

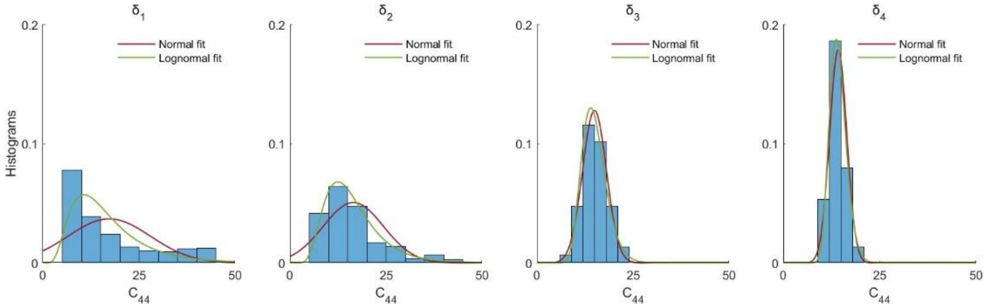

Figure 14: Fitting of both the normal and the lognormal distribution to the histograms of the elasticity component C_{44}.

3 RESPONSE VARIABILITY OF CONCRETE STRUCTURES

This section focuses on generating sample functions of the random fields of the elasticity tensor of concrete by applying the spectral representation method in conjunction with the mathematical theory of translation fields. This method is well suited in the context of Monte Carlo simulation, which is used for computing the response variability of two concrete structures [11]. Useful conclusions are derived regarding the effect of the random microstructure on the macroscopic behavior of concrete.

3.1 Spectral representation method

The i-th sample function of a two-dimensional homogeneous Gaussian field is given by [4]:

$$f^{(i)}(x,y)=\sqrt{2}\sum_{n_x=0}^{N_x-1}\sum_{n_y=0}^{N_y-1}\Big[A^{(1)}_{n_xn_y}\cos\left(\kappa_{xn_x}x+\kappa_{yn_y}y+\varphi^{(1)(i)}_{n_xn_y}\right) + A^{(2)}_{n_xn_y}\cos\left(\kappa_{xn_x}x-\kappa_{yn_y}y+\varphi^{(2)(i)}_{n_xn_y}\right)\Big] \tag{13}$$

where $\varphi^{(1)(i)}_{n_xn_y},\varphi^{(2)(i)}_{n_xn_y}$ the i-th sample of the independent random phase angles uniformly distributed in the range $[0,2\pi]$. The coefficients $A^{(1)}_{n_xn_y}$, $A^{(2)}_{n_xn_y}$ are written as:

$$A^{(1)}_{n_xn_y}=\sqrt{2S_{ff}\left(\kappa_{xn_x},\kappa_{yn_y}\right)\Delta\kappa_x\Delta\kappa_y} \tag{14}$$

$$A^{(2)}_{n_xn_y}=\sqrt{2S_{ff}\left(\kappa_{xn_x},-\kappa_{yn_y}\right)\Delta\kappa_x\Delta\kappa_y} \tag{15}$$

where

$$\kappa_{xn_x} = n_x \Delta\kappa_x \qquad \kappa_{yn_y} = n_y \Delta\kappa_y \tag{16}$$

$$\Delta\kappa_x = \frac{\kappa_{xu}}{N_x} \qquad \Delta\kappa_y = \frac{\kappa_{yu}}{N_y} \tag{17}$$

$$n_x = 0,1,..., N_x - 1 \qquad n_y = 0,1,..., N_y - 1 \tag{18}$$

and

$$A^{(1)}_{0n_y} = A^{(1)}_{n_x 0} = 0 \tag{19}$$

$$A^{(2)}_{0n_y} = A^{(2)}_{n_x 0} = 0 \tag{20}$$

or

$$S_{ff}\left(0, \kappa_y\right) = S_{ff}\left(\kappa_x, 0\right) = 0 \tag{21}$$

The terms N_x, N_y represent the number of intervals in which the wave number axes are subdivided, while the terms κ_{xu}, κ_{yu} represent the cut-off wave numbers beyond which the power spectral density function of the random field is assumed to be zero. The cut-off wave numbers are computed as:

$$\int_{0}^{\kappa_{xu}} \int_{-\kappa_{yu}}^{\kappa_{yu}} S_{ff}\left(\kappa_x, \kappa_y\right) d\kappa_x d\kappa_y = \left(1-\varepsilon\right) \int_{0}^{\infty} \int_{-\infty}^{\infty} S_{ff}\left(\kappa_x, \kappa_y\right) d\kappa_x d\kappa_y \tag{22}$$

where ε an arbitrarily small positive number, such as $\varepsilon = 0.001$.

The fulfillment of Equations (19)-(21) is necessary to ensure that the mean value and auto-correlations of any sample function are identical to those of the original field. Additionally, to avoid the aliasing effect, the space increments Δx and Δy, separating the generated values of any sample function along the x, y axes respectively, must satisfy the conditions:

$$\Delta x \le \frac{\pi}{\kappa_{xu}} \qquad \Delta y \le \frac{\pi}{\kappa_{yu}} \tag{23}$$

The power spectral density function corresponding to the squared exponential model is given by:

$$S_{ff}\left(\kappa_x, \kappa_y\right) = \sigma^2 \frac{b_x b_y}{4\pi} \exp\left[-\left(\frac{b_x \kappa_x}{2}\right)^2 - \left(\frac{b_y \kappa_y}{2}\right)^2 \right] \tag{24}$$

It is noted that the same set of phase angles was used for generating the sample functions of the elasticity components C_{11} and C_{44}. This is in accordance with the observation that the elasticity components C_{11} and C_{44} exhibit a strong correlation with each other. The terms N_x, N_y were selected equal to 20.

3.2 Translation fields

The generation of sample functions of a non-Gaussian field is based on a simple transformation of some underlying Gaussian field. If $g(x,y)$ a homogeneous zero-mean Gaussian field with unit variance, then a homogeneous non-Gaussian field $f(x,y)$ is defined as:

$$f(x,y) = F^{-1}\Phi\lfloor g(x,y)\rfloor \tag{25}$$

where Φ the standard Gaussian cumulative distribution function and F the non-Gaussian marginal cumulative distribution function of $f(x,y)$. The transformation $F^{-1}\Phi$ is a memory-less translation, since the value of $f(x,y)$ at an arbitrary point (x,y) depends on the value of $g(x,y)$ at the same point only. The resulting non-Gaussian field is called a translation field [5].

In the case of lognormal translation fields, Equation (25) becomes:

$$f(x,y) = \exp\lfloor \mu + \sigma g(x,y)\rfloor \tag{26}$$

where μ and σ the auxiliary parameters of the transformation.

3.3 Monte Carlo simulation

In the Monte Carlo simulation method, $NSIM$ samples of a deterministic problem are generated and the problem is then solved as many times as the number of samples. The response variability of the problem is determined using well-known relationships of statistics. For example, the mean value and variance of the displacement u_i at degree of freedom i are computed as:

$$E(u_i) = \frac{1}{NSIM}\sum_{j=1}^{NSIM} u_i(j) \tag{27}$$

$$\sigma^2(u_i) = \frac{1}{NSIM-1}\left\lfloor \sum_{j=1}^{NSIM} u_i^2(j) - NSIM\, E^2(u_i)\right\rfloor \tag{28}$$

It is obvious that the accuracy of the estimation depends on the number of samples, which was selected equal to 1000.

3.4 Numerical examples

In this section, the generated sample functions of the elasticity components C_{11} and C_{44} are compared with the original fields and the response variability of two concrete structures is examined. More specifically, the analyzed structures include a simply supported and a cantilever beam subject to a uniform and a concentrated load respectively.

3.4.1 Generated sample functions

Figures 15a and 16a depict the generated sample functions of the elasticity components C_{11} and C_{44} in the same domain as the original fields, while Figures 15b and 16b depict their auto-correlations for lag values along x (ξ_x, $\xi_y = 0$) and y ($\xi_x = 0$, ξ_y). It is observed that the first two statistical moments and the auto-correlations of the sample functions of the elasticity components C_{11} and C_{44} are almost identical to those of the original fields.

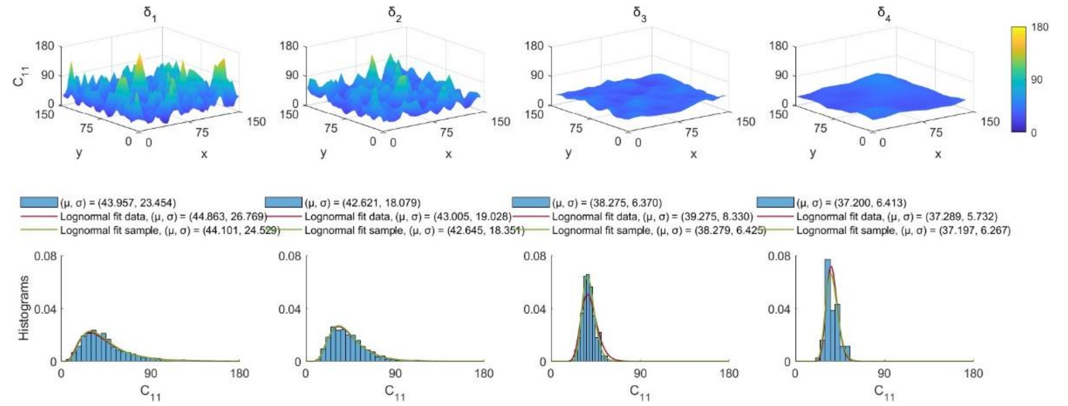

Figure 15a: Generated sample functions of the elasticity component C_{11}.

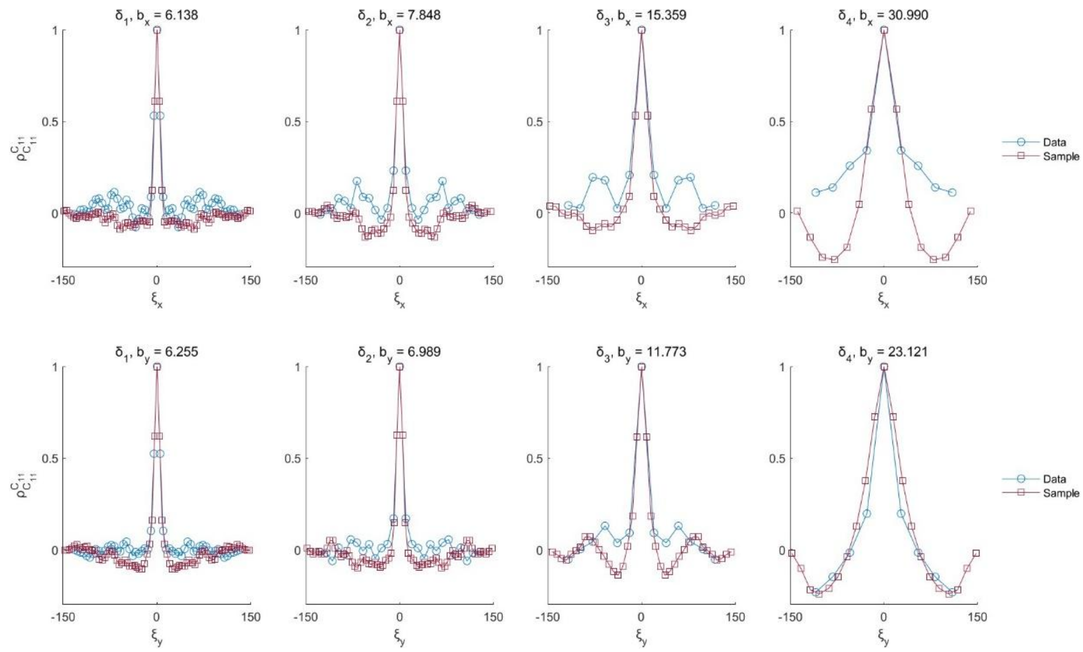

Figure 15b: Auto-correlations of the elasticity component C_{11} for lag values along x (ξ_x , $\xi_y = 0$) and y ($\xi_x = 0$, ξ_y).

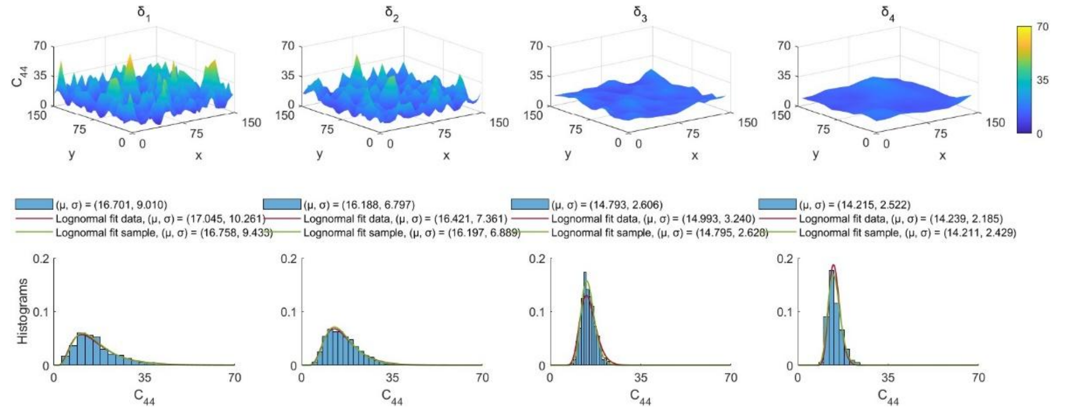

Figure 16a: Generated sample functions of the elasticity component C_{44}.

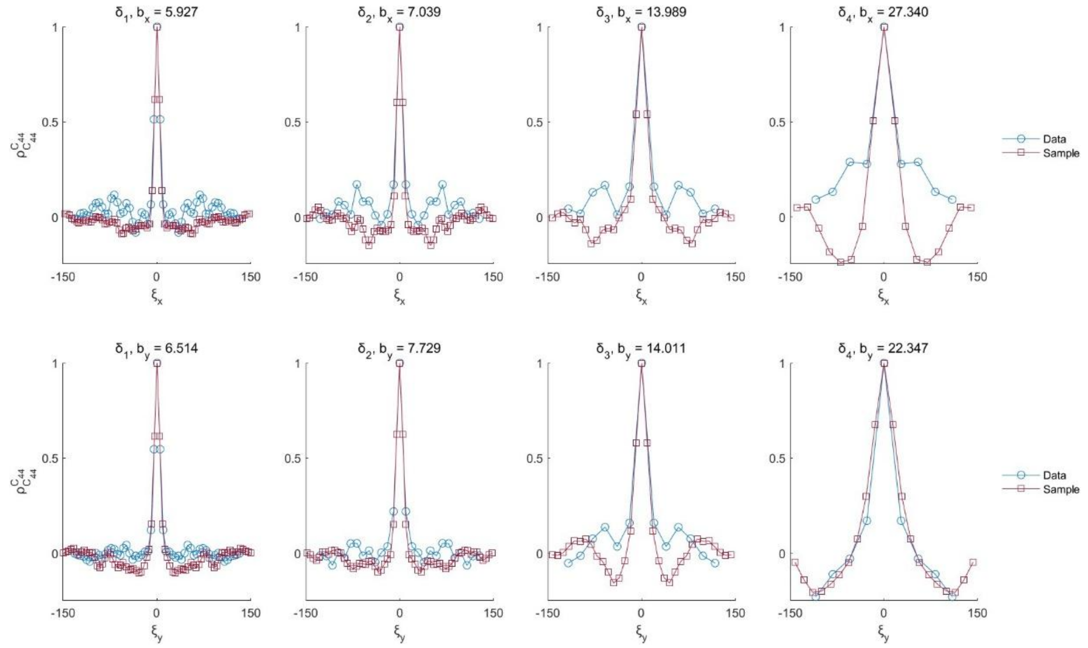

Figure 16b: Auto-correlations of the elasticity component C_{44} for lag values along x (ξ_x , $\xi_y = 0$) and y ($\xi_x = 0$, ξ_y).

3.4.2 Simply supported beam

The simply supported beam analyzed is depicted in Figure 17. The beam has a unit thickness and is modeled with four-node quadrilateral isoparametric elements under plane stress conditions. The element size is chosen between $b/4$ and $b/2$ with $b = \min\left(b_x, b_y\right)$, to sufficiently capture the variation of the random fields of the elasticity components C_{11} and C_{44} . The generated values of the sample functions correspond to the centroids of the elements. It is noted that the monitored response quantity is the vertical displacement u_y at the midpoint of the bottom edge of the beam.

The mean and COV of the displacement u_y are plotted in Figure 18 with respect to the number of Monte Carlo simulations, along with the response histogram. Statistical convergence of the results is achieved and it is observed that the structural response is influenced by the statistical characteristics of the random fields of the elasticity components C_{11} and C_{44} and particularly by the examined mesoscale sizes.

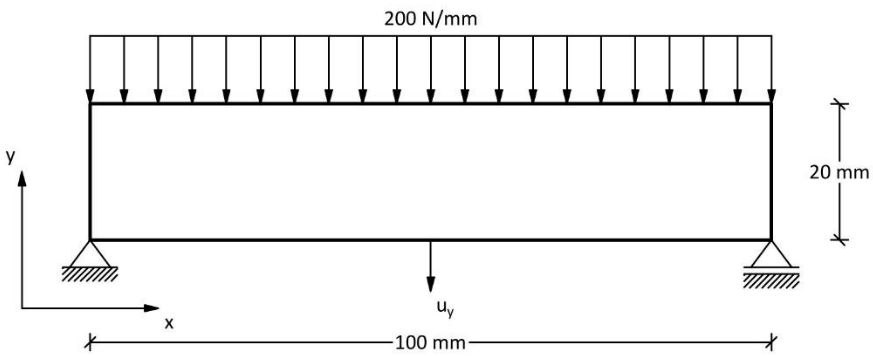

Figure 17: Simply supported beam subject to a uniform load.

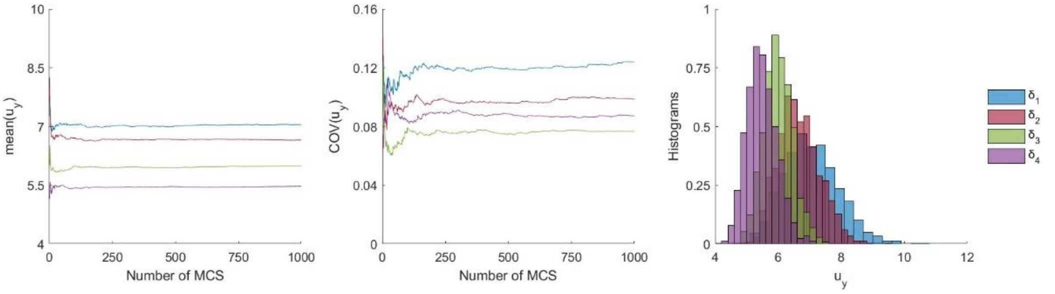

Figure 18: Mean and COV of the displacement u_y with respect to the number of Monte Carlo simulations, along with the response histogram.

3.4.3 Cantilever beam

The cantilever beam analyzed is depicted in Figure 19. The beam has a unit thickness and is modeled with four-node quadrilateral isoparametric elements under plane stress conditions. As in the previous example, the element size is chosen between $b/4$ and $b/2$ with $b = \min\left(b_x, b_y\right)$, to sufficiently capture the variation of the random fields of the elasticity components C_{11} and C_{44}. The generated values of the sample functions correspond to the centroids of the elements. It is noted that the monitored response quantity is the vertical displacement u_y at the free end of the bottom edge of the beam.

The mean and COV of the displacement u_y are plotted in Figure 20 with respect to the number of Monte Carlo simulations, along with the response histogram. Statistical convergence of the results is achieved and it is again observed that the structural response is influenced by the statistical characteristics of the random fields of the elasticity components C_{11} and C_{44} and particularly by the examined mesoscale sizes.

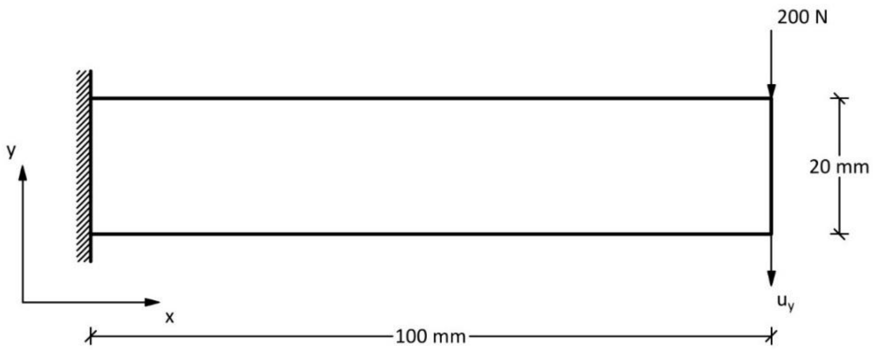

Figure 19: Cantilever beam subjected to a concentrated load.

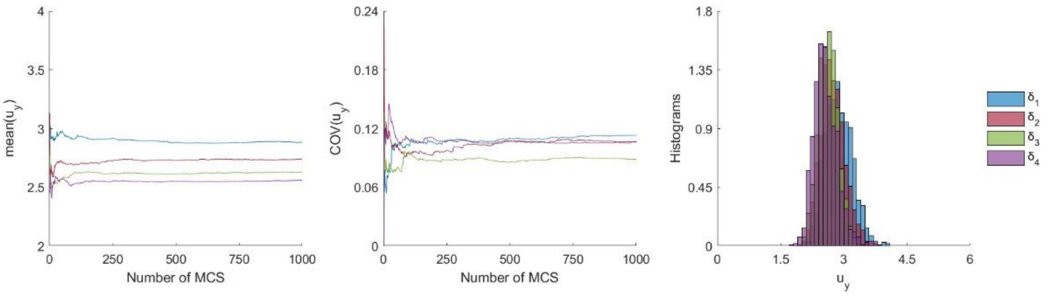

Figure 20: Mean and COV of the displacement u_y with respect to the number of Monte Carlo simulations, along with the response histogram.

4 CONCLUSIONS

In this work, the mesoscale random fields of the elasticity tensor of concrete were determined by applying the moving window method to the reconstructed microstructure of a cubic specimen. Additionally, their statistical characteristics were computed and the methodology for generating sample functions was described, in order to examine the response variability of two concrete structures and to understand the effect of the random microstructure on their macroscopic behavior. The key conclusions derived are as follows:

- The random fields of the elasticity components C_{11} and C_{44} become less variable and histograms narrower, as the scale factor increases. More specifically, the COV reduces from 63% to 16% for both elasticity components C_{11} and C_{44}, as the scale factor increases.
- The elasticity components C_{11} and C_{44} exhibit a strong correlation with each other, as expected.
- The correlation lengths of the random fields of the elasticity components C_{11} and C_{44} increase, as the scale factor increases. In other words, the random fields tend to a random variable, as the scale factor increases.
- The random fields of the elasticity components C_{11} and C_{44} are statistically isotropic at smaller scales, whereas a slight deviation from statistical isotropy is observed at larger scales.
- The elasticity components C_{11} and C_{44} are well described by the lognormal distribution.
- The first two statistical moments and the auto-correlations of the sample functions of the elasticity components C_{11} and C_{44} are almost identical to those of the original fields.
- The selected number of samples is sufficient to achieve statistical convergence of the results.
- The structural response is influenced by the statistical characteristics of the random fields of the elasticity components C_{11} and C_{44} and particularly by the examined mesoscale sizes.
- The response COV tends approximately to the COV of both elasticity components C_{11} and C_{44} at larger scales [3], while a reduction with respect to the input uncertainty is observed at smaller scales.

The combination of the above observations can lead to safer and more cost-effective design of concrete structures, as well as to the improvement of safety factors in construction codes. The consideration of the interfacial transition zone for determining the spatial variation of the elastic properties of concrete and the conduction of experiments to select the appropriate scale factor [12] are subjects of further research that will contribute even more in this direction.

ACKNOWLEDGEMENTS

The financial support provided by the John S. Latsis Public Benefit Foundation scholarship for Leontios Kotropoulos' postgraduate studies during the academic year 2024-2025 is gratefully acknowledged.

REFERENCES

[1] P. Wriggers & S. O. Moftah, "Mesoscale models for concrete: Homogenisation and damage behaviour", *Finite Elements in Analysis and Design*, vol. 42, no. 7, pp. 623-636, 2006. https://doi.org/10.1016/j.finel.2005.11.008

[2] G. Stefanou, D. Savvas & P. Metsis, "Random Material Property Fields of 3D Concrete Microstructures Based on CT Image Reconstruction", *Materials*, vol. 14, no. 6, p. 1423, 2021. https://doi.org/10.3390/ma14061423

[3] G. Stefanou, D. Savvas & M. Papadrakakis, "Stochastic finite element analysis of composite structures based on mesoscale random fields of material properties", *Computer Methods in Applied Mechanics and Engineering*, vol. 326, pp. 319-337, 2017. https://doi.org/10.1016/j.cma.2017.08.002

[4] M. Shinozuka & G. Deodatis, "Simulation of Multi-Dimensional Gaussian Stochastic Fields by Spectral Representation", *Applied Mechanics Reviews*, vol. 49, no. 1, pp. 29-53, 1996. https://doi.org/10.1115/1.3101883

[5] M. Grigoriu, "Simulation of Stationary Non-Gaussian Translation Processes", *Journal of Engineering Mechanics*, vol. 124, no. 2, 1998. https://doi.org/10.1061/(ASCE)0733-9399(1998)124:2(121)

[6] Z. Hashin, "Analysis of Composite Materials – A Survey", *Journal of Applied Mechanics*, vol. 50, no. 3, pp. 481-505, 1983. https://doi.org/10.1115/1.3167081

[7] R. Hill, "Elastic properties of reinforced solids: Some theoretical principles", *Journal of the Mechanics and Physics of Solids*, vol. 11, no. 5, pp. 357-372, 1963. https://doi.org/10.1016/0022-5096(63)90036-X

[8] D. Savvas, G. Stefanou & M. Papadrakakis, "Determination of RVE size for random composites with local volume fraction variation", *Computer Methods in Applied Mechanics and Engineering*, vol. 305, pp. 340-358, 2016. https://doi.org/10.1016/j.cma.2016.03.002

[9] M. Ostoja-Starzewski, S. Kale, P. Karimi, A. Malyarenko, B. Raghavan, S. I. Ranganathan & J. Zhang, "Chapter Two – Scaling to RVE in Random Media", *Advances in Applied Mechanics*, vol. 49, pp. 111-211, 2016. https://doi.org/10.1016/bs.aams.2016.07.001

[10] C. Miehe & A. Koch, "Computational micro-to-macro transitions of discretized microstructures undergoing small strains", *Archive of Applied Mechanics*, vol. 72, pp. 300-317, 2002. https://doi.org/10.1007/s00419-002-0212-2

[11] G. Stefanou, "The stochastic finite element method: Past, present and future", *Computer Methods in Applied Mechanics and Engineering*, vol. 198, no. 9-12, pp. 1031-1051, 2009. https://doi.org/10.1016/j.cma.2008.11.007

[12] G. Stefanou, D. Savvas, P. Gavallas & I. Papaioannou, "The effect of random field parameter uncertainty on the response variability of composite structures", *Composites Part C: Open Access*, vol. 9, p. 100324, 2022. https://doi.org/10.1016/j.jcomc.2022.100324